Journal of Power Sources 376 (2018) 82–90

Contents lists available at ScienceDirect

Journal of Power Sources

journal homepage: www.elsevier.com/locate/jpowsour

Biochar-based carbons with hierarchical micro-meso-macro porosity for high rate and long cycle life supercapacitors

Zhipeng Qiu[a], Yesheng Wang[a], Xu Bi[a], Tong Zhou[b], Jin Zhou[a,*], Jinping Zhao[a], Zhichao Miao[a], Weiming Yi[c], Peng Fu[c], Shuping Zhuo[a]

[a] School of Chemistry and Chemical Engineering, Shandong University of Technology, Zibo 255049, PR China
[b] Lab of Functional Molecules and Materials, School of Physics and Optoelectronic Engineering, Shandong University of Technology, Zibo 255049, PR China
[c] School of Agricultural Engineering and Food Science, Shandong University of Technology, Zibo 255049, PR China

HIGHLIGHTS

- The corn straw biochar is used as precursor for preparation of porous carbon.
- The biochar-based carbons possess typical hierarchical porosity.
- The BBC-4 carbon exhibits high rate performance and outstanding cyclic stability.
- BBC-4 carbon could steady work at 1.6 V in Na_2SO_4 electrolyte over 3000 cycles.

GRAPHICAL ABSTRACT

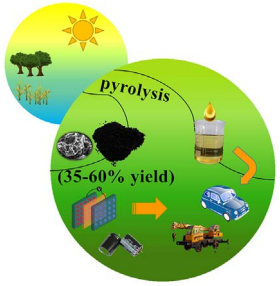

ARTICLE INFO

Keywords:
Supercapacitor
Carbon materials
Biochar
Hierarchial porous carbon
Pyrolysis
KOH activation

ABSTRACT

The development of supercapacitors with high energy density and power density is an important research topic despite many challenging issues exist. In this work, porous carbon material was prepared from corn straw biochar and used as the active electrode material for electric double-layer capacitors (EDLCs). During the KOH activation process, the ratio of KOH/biochar significantly affects the microstructure of the resultant carbon, which further influences the capacitive performance. The optimized carbon material possesses typical hierarchical porosity composed of multi-leveled pores with high surface area and pore volume up to 2790.4 $m^2 g^{-1}$ and 2.04 $cm^3 g^{-1}$, respectively. Such hierarchical micro-meso-macro porosity significantly improved the rate performance of the biochar-based carbons. The achieved maximum specific capacitance was 327 F g^{-1} and maintained a high value of 205 F g^{-1} at a ultrahigh current density of 100 A g^{-1}. Meanwhile, the prepared EDLCs present excellent cycle stability in alkaline electrolytes for 120 000 cycles at 5 A g^{-1}. Moreover, the biochar-based carbon could work at a high voltage of 1.6 V in neutral Na_2SO_4, and exhibit a high specific capacitance of 227 F g^{-1}, thus giving an outstanding energy density of 20.2 Wh kg^{-1}.

1. Introduction

The development of new and efficient energy storage devices is a critical component of utilization of sustainable energy. Supercapacitors [1], lithium ion batteries [2] and some other rechargeable batteries [3,4] are considered to be promising energy storage devices. In particular, the supercapacitors have got lots of attentions due to their exceptional power density, ultra-long cycle life, good convertibility and extensive storage applications prospects [5–7]. According to the work mechanism, supercapacitor could be divided into pseudo-capacitors

* Corresponding author.
E-mail address: zhoujin@sdut.edu.cn (J. Zhou).

https://doi.org/10.1016/j.jpowsour.2017.11.077
Received 24 August 2017; Received in revised form 1 November 2017; Accepted 24 November 2017
Available online 28 November 2017
0378-7753/

and electrochemical double layer capacitors (EDLCs). Pseudo-capacitive materials, such as transition metal oxides, conductive polymer and their composites, store energies by reversible redox reaction of the electroactive species, and could give very high specific capacitance. However, these electrode materials generally possess poor cycle performance, low conductivity and high price. Moreover, the pseudo-capacitive materials are always used to asymmetric supercapacitors matching with a carbon electrode materials. The above facts limit the practical application of these materials. Differently, EDLCs store energies by the electrostatic charge uptake at the electrolyte/electrode interfacial regions, and exhibit superior long-term cycle performance.

However, the much low energy densities (approximately 5 Wh kg^{-1}) of commercial EDLCs have hindered their wide applications [8,9]. In order to improve performance and expand application fields, researchers are exploring new electrode materials for supercapacitors. Porous carbons have recently aroused great passion due to their large surface area, stable chemical properties, high conductivity, cheap, availability and structure adjustable [10].

Generally, the performance of carbon materials in EDLCs is highly dependent on the migration and adsorption of ions inside nanopores, which are largely determined by the pore structure of the material. Porous structure could be designed and developed by many methods, such as physical [11] or chemical activation [12], polymer blend carbonization [13], soft template [14] and hard template [15] associated with carbonization or activation [16]. Chemical activation is an effective and low-cost way to develop porous structure, which operate at lower temperature and in shorter activation time. KOH [17–20], NaOH [21], H_3PO_4 [22] and $ZnCl_2$ [23] are generally selected as activation agents for chemical activation.

In recent years, waste biomass, such as abandoned coffee beans [24], starch [25], apricot shell waste [26], sugarcane bagasse [27–29], rice husk [30], peanut shell [31], wood [32], potato starch [33] and rubber wood sawdust [34], as precursors in the preparation of carbon materials for EDLCs have gained much attention due to their huge reserves and economical [35]. Generally, residual biomass accounts for 10% of the global energy storage [36]. According to full estimate, the potential of annual biomass is predicted to be as high as 1.08×10^{11} toe (tons of oil equivalent), which is almost 10 times of the world's current energy requirement [37,38]. The large-scale utilization of biomass resources can largely ease the fossil crisis, which has become the major driver of the biomass energy research. We can stored this energy by biomass pyrolysis to produce biomass fuels which can be readily transported and effectively utilized. The product of biomass pyrolysis were biodiesel, biochar, and gas [39,40]. The biochar is the main solid product which has a large yield about 35–60 wt% [36,41]. The applications of biochar contain adsorbent, soil fertilizer and agricultural by-product/waste recycling [42]. Considering the broad scale of supercapacitor utilizations, developing carbon electrode materials from renewable biochar is of high application prospects [43].

In this work, the corn straw biochar are used to be prepared porous carbon materials for high performance supercapacitors. As shown in Fig. 1, the biochar are prepared by a flash pyrolysis of corn straw which is one of most common straws in north China. After a KOH activation process, biochar-based porous carbons (BBCs) are prepared. These carbons are proved to possess typical hierarchial porosity composed of multi-leveled pores. The prepared BBCs samples are applied as electrodes materials of supercapacitor, and show excellent capacitive performance in aqueous electrolytes (6 M KOH, 1 M H_2SO_4 and 1 M Na_2SO_4 electrolyte): a very high specific capacitance up to 327 F g^{-1}, outstanding rate performance with a high specific capacitance of 205 F g^{-1} at 100 A g^{-1}, high work voltage up to 1.6 V and ultrahigh energy density of 20.2 Wh kg^{-1} in neutral electrolyte, and impressive long-term stability up to 120 000 cycles.

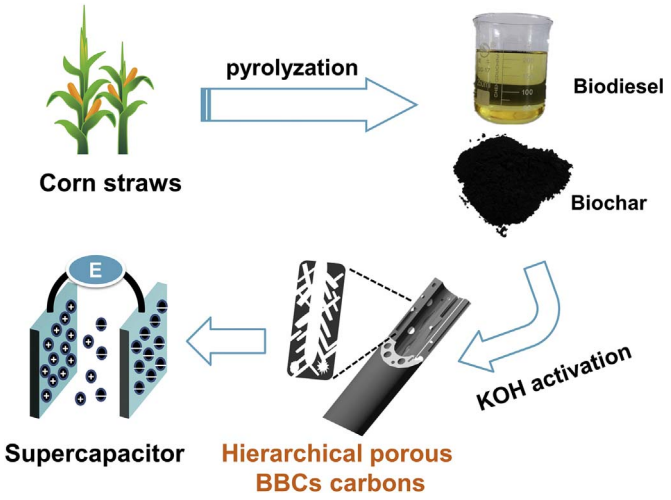

Fig. 1. Illustration for biochar-based porous carbon materials.

2. Experimental section

2.1. Material preparation

Corn straws are gathered from farmland of north China and thoroughly washed to remove impurities. All the chemical reagent, including KOH, Na_2SO_4, H_2SO_4 and polytetrafluoroethylene (PTFE) emulsion etc. are analytical pure and are purchased from Sinopharm Chemical Reagent Co., Ltd. The pyrolysis reactor was a home-made fluidized bed, which can heat corn straw in an inert atmosphere. The biochar were obtained as a solid residue in a yield about 40% via a flash pyrolysis of corn straws on a home-made fluidized bed at a temperature of 450 °C. Biodiesel was collected in a beaker and the separated biochar was the raw material in this study [44].

The biochar-based carbons were prepared from corn straw biochar via a KOH activation method. The typical procedure of biochar-based carbons is that: 100–200 mesh of biochar powder are firstly mixed with different proportion of KOH and small amount of H_2O. The use of H_2O is to dissolve the KOH and obtain an even mixture of KOH with the biochar. The obtained mixture was placed in carbonization furnace tube, heated to 800 °C at a heating rate of 5 °C min^{-1} under N_2 flow, and further maintained for 1 h. After cooling down to the room temperature, the black solid residue were repeatedly washed by 1 M HF, 1 M HCl and distilled water to be neutral. For convenience, the prepared carbon samples are named as BBC-x, in which BBC and x stand for biochar-based carbon and the weight ratio of KOH/biochar (1, 2, 3 and 4), respectively.

2.2. Material characterization

Micro morphology of the BBC-x were observed by scanning electron microscope (SEM, Sirion 200 FEI, Netherlands) and transmission electron microscope (TEM, JEM2100, JEOL, Japan). Element composition and their atom binding states were characterized by energy dispersive spectroscopy (EDS, INCA Energy spectrometer, Netherlands) and a X-ray photoelectron spectroscopy (XPS, Escalab 250, USA). X-ray diffraction (XRD) patterns of the carbon materials were conducted on a Brucker D8 Advance diffractometer with Cu Kα radiation. Raman spectra were collected by a LabRAM HR800 from JY Horiba. The electronic conductivity was measured by a ST-2722 Semiconductor resistivity tester (Lattice Electronics Co. Ltd., Suzhou, China). And the data of electronic conductivity was calculated from the average of three measurements. The porosity of the prepared carbon materials was analyzed by an ASAP 2020 nitrogen sorption system (Micrometitics, USA). The carbon materials were degassed at 350 °C for 4 h before

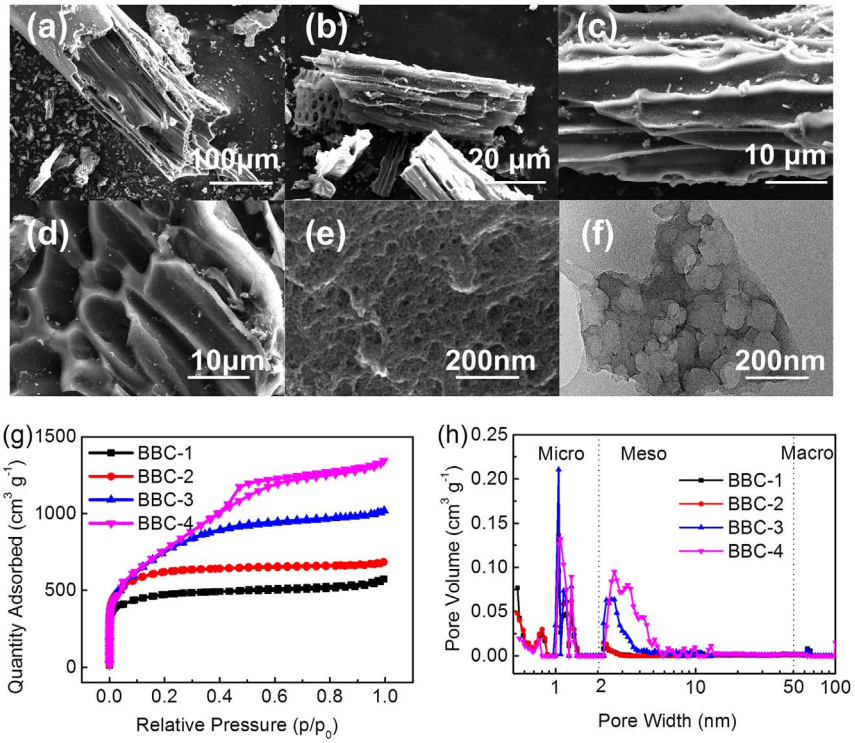

Fig. 2. (a–c) SEM images of the raw biochar, (d, e) SEM images of BBC-4, (f) TEM image of BBC-4, (g) nitrogen sorption isotherms and (h) pore size distribution plots of the biochar-based carbons.

sorption measurements. Brunauer-Emmett-Teller (BET) surface area (S_{BET}) was calculated from the N_2 adsorption isotherm data within the relative pressure (p/p_0) of 0.05–0.25. Total pore volume (V_T) was obtained at a relative pressure of 0.995. Micropore surface area (S_{micro}) and volume (V_{micro}) were calculated by t-plot method. Mesopore surface area (S_{meso}) and volume (V_{meso}) were calculated by subtracting the micropore surface area and volume from the BET surface area and total pore volume, respectively. Pore size distributions (PSDs) were obtained from the adsorption isotherms by using the nonlocal density functional theory (NLDFT) model and assuming a slit-shape pore.

2.3. Electrochemical test

Working electrodes were made by pressing a mixture of the studied carbons and polytetrafluoroethylene (PTFE) binder with a weight ratio of 95:5 onto the collectors under 10 MPa. The mass loading and geometric area of the electrode material on the work electrode is about 2 mg and 0.25 cm^2 (0.5 × 0.5 cm), respectively, responding to about 8 mg cm^{-2}. The thickness of electrode is about 200 μm, as shown in the SEM image of the work electrode in the KOH electrolyte (Fig. S1). This thickness may be underestimated because the electrode materials may be pressed into the framework of nickel foam. In the alkaline electrolyte, nickel foam was used as the collector, while titanium mesh was used in H_2SO_4 and Na_2SO_4 electrolyte.

The electrochemical performances of the prepared carbons were studied on a CHI660D electrochemical testing station (Chenhua Instruments Co. Ltd., Shanghai). All electrochemical test, including cyclic voltammetry (CV) and galvanostatic charge/discharge (GCD), were performed in a two-electrode system which are fabricated by two work electrodes and a sandwiched cellulose separator. All the electrodes and electrolytes were vacuumed to avoid side reactions between the carbon based electrodes and O_2 dissolved in the solution. The GCD test was used to determine the specific capacitance at a certain current density. In this work, the charge/discharge current density was controlled in the range of 0.2–100 A g^{-1} for 6 M KOH electrolyte, 0.2–60 A g^{-1} for 1 M H_2SO_4 electrolyte, 0.2–60 A g^{-1} for 1 M Na_2SO_4 electrolyte. For the long-term cyclic charge/discharge test, a 2032 coin battery was used in the case of KOH electrolyte, while a closed system was made by encapsulating two titanium mesh work electrodes, separator and proper amount of electrolyte in a plastic bag sealed by a plastic film sealer in the case of H_2SO_4 and neutral electrolytes. The long-term GCD experiments were carried out on an automatic galvanostatic charge/discharge unit (Land CT 2001 A, Wuhan, China) at a current density of 5 A g^{-1}.

The specific capacitance of the prepared carbons was calculated from the galvanostatic charge/discharge test at different current density, by the following formula:

$$C_m = \frac{4I \times t}{\Delta V \times m} \quad (1)$$

Where C_m (F g^{-1}) is the gravimetric specific capacitance of the carbon materials, I (A) and t (s) is the discharge current and the discharge time, ΔV (V) is the voltage window, and m (g) is the mass of active material loading on two working electrodes, respectively. The energy density (E) and powder density (P) of the investigated carbon materials could be calculated from the galvanostatic charge/discharge test using the following equations:

$$E = \frac{1}{8} \times C_m \times V^2 \quad (2)$$

$$P = \frac{E}{t} \quad (3)$$

where the C_m, V and t are the specific capacitance of the carbons, discharge voltage decrease and discharge time, respectively.

3. Results and discussions

3.1. Materials characterization

Fig. 2 and S2 shows the SEM and TEM observations of the raw biochar, BBC-1 and BBC-4 samples, nitrogen sorption isotherms and pore size distribution (PSD) plots of BBCs materials. As shown in Fig. 2a–c, the raw biochar keep corn straw's original fibrous structure with a large-sized through tubular channels in the process of producing

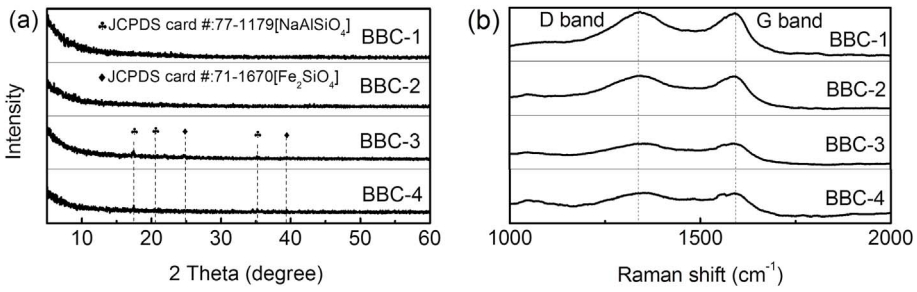

Fig. 3. (a) XRD patterns and (b) Raman spectra of the BBCs samples.

biodiesel. For BBC-1, many big holes on the surface after KOH activated, but no apparent nanopores are observed from high resolution SEM images indicating that the porosity of this carbon is mainly consisted of micropores (Fig. S2a, b). As shown in Fig. 2d and e, it could be also found that BBC-4 is polyporous. From the high-magnification SEM images of the wall of tubular channels (Fig. 2e and S2d), the carbon surface becomes much rougher with the increasing of KOH dosage, and a number of large-sized mesopores are observed for BBC-4, indicating that the activation degree increases as the KOH dosage increases. TEM images further confirms the existence of these pores on the wall of the tubular channels (Fig. 2f). High resolution TEM observations shows that lots of worm-like micropores are developed in the prepared carbon materials (Fig. S2f, g). The results of SEM and TEM observation indicate that the KOH activation generated a lot of mesopores on the fiber wall and lots of micropores on the mesopores wall, but did not destroy porous fibrous skeleton.

High-performance carbon electrode materials of supercapacitor usually depend on their large specific surface area and high-developed nanoporosity. We further performed N_2 sorption measurements to determine the pore texture and specific surface area (Fig. 3), calculated pore size distributions (PSDs) of the prepared carbons. No valid sorption data are collected for the biochar, indicating the raw material is typically non-porous. As shown in Fig. 2g, the isotherms of BBC-1, BBC-2, BBC-3 show features of type I isotherm. BBC-4 shows obvious characteristic of type IV isotherm. With the dosage of KOH increasing, the adsorption quantities and specific surface area significant accrue. All the four samples are rapidly saturated at low relative pressure, indicating the adsorption in plenty of micropores. BBC-4 presented a slight increase of sorption capacity and a hysteresis loop when the relative pressure approaches to 0.5, indicating the existence of plenty mesopores larger than 2 nm. Comparatively, no obviously sorption capacity is detected for the other three carbons at a high relative pressure, indicating only a small number of large pores exist in carbon skeletons. The PSDs plotted in Fig. 2h further confirm the above facts. The typical porosity parameters of BBCs are summarized in Table 1. It can be seen that the specific surface areas and the pore volume of the prepared carbons significantly increase as the KOH dosage increases. The specific surface area and pore volume of BBC-4 is 2790.4 $m^2\ g^{-1}$ and 2.04 $cm^3\ g^{-1}$, respectively, which is much higher than the others. It is also been seen that S_{meso} and V_{meso} significantly increases with the increasing of KOH dosage, while those values of micropores firstly increase and then decrease. This fact indicates that more micropores are activated under the KOH/biochar weight ratio of 2, and many micropores collapse and ultimately merge into larger mesopores when the KOH/biochar weight ratio further increases. Combination the results of the electronic microscopy and N_2 sorption, it could be concluded that biochar derived BBC-4 has a typical hierarchical porosity, which is made up of a certain amount of micropores (< 2 nm), large number of mesopores (2–10 nm), some macropores and macroscopic tubular holes. This hierarchical pore texture not only improves the surface area greatly, but also makes it easier for electrolyte ions to diffuse from external electrolyte into the internal space of electrode materials, thus leading to excellent capacitive performance, such as high specific capacitance, good rate performance, and so on.

The KOH activation is a proverbial method to produce pore structure in carbons, its mechanism has been well understood by a large number of experimental studies [45–48]. According to the previous studies, in the process of KOH activation, the KOH (mp. 360 °C) is firstly melted and sufficiently contacts with the carbon precursor. The redox reaction between molten KOH and carbon precursor starts at around 400 °C, forming K_2CO_3. At about 600 °C, KOH is completely consumed and were totally transformed into K_2CO_3. At temperatures higher than 700 °C, the as-formed K_2CO_3 in Equation (4) began to decomposing into CO_2 and K_2O (Equation (5)), completely disappears at 800 °C. Moreover, the resulting CO_2 can be further reduced by carbon to form CO at high temperature (Equation (6)). The K compounds (K_2O and K_2CO_3) also can be reduced by carbon to produce metallic K at temperatures over 700 °C (Equations (7) and (8)). The alkali metals become vapour with high diffusivity, and easily intercalate into the carbon lattices, thus resulting much developed microporosity [47].

$$6KOH + 2C \rightarrow 2K + 3H_2 + 2K_2CO_3 \quad (4)$$

$$K_2CO_3 \rightarrow K_2O + CO_2 \quad (5)$$

$$CO_2 + C \rightarrow 2CO \quad (6)$$

$$K_2CO_3 + 2C \rightarrow 2K + 3CO \quad (7)$$

$$C + K_2O \rightarrow 2K + CO \quad (8)$$

The biochar and BBCs are further analyzed by XRD measurements. As shown in Fig. S3, a series of sharp peaks at 2θ = 20.45, 26.56, 36.47, 39.31, 49.96, and 54.83° are present on the XRD pattern of the biochar, indicating the existence of hexagonal α-SiO_2 (JCPDS card #:81-0065). Additionally, a broad peaks centered at 25.67° is also observed, responding to the diffraction of (002) lattice plane of graphite. However, this peak is very weak due to incomplete pyrolysis of corn straw at the

Table 1
Porosity parameters and conductivity of the prepared carbons.

Sample	$S_{BET}/m^2\ g^{-1}$	$S_{micro}/m^2\ g^{-1}$	$S_{meso}/m^2\ g^{-1}$	$V_t/cm^3\ g^{-1}$	$V_{micro}/cm^3\ g^{-1}$	$V_{meso}/cm^3\ g^{-1}$	Conductivity/mS cm^{-1}
BBC-1	1475.3	1294.9	180.4	0.87	0.65	0.22	33
BBC-2	1936.9	1732.7	204.3	1.04	0.87	0.17	40
BBC-3	2636.2	1365.5	1270.7	1.55	0.62	0.93	26
BBC-4	2790.4	568.4	2221.6	2.04	0.08	1.96	23

low pyrolysis temperature of 450 °C. As shown in the XRD pattern of BBCs (Fig. 3a), most of SiO_2 have been removed by repeatedly washing with HF, HCl and distilled water after KOH activation. However, several impure peaks at 17.47, 20.47, 24.77, 34.52, 35.17, and 51.10° are observed (Fig. 3a, S3b). It is believed that these peaks are produced by the inorganic composition of the BBC-4 carbon. We burned BBC-4 carbon at a muffle furnace at 800 °C and obtained a grey ash (about 5 wt%). According to EDS analysis, the ash is mainly consisted of Fe (15 at.%), Si (3 at.%), Na (5 at.%), C (25 at.%), O (50 at.%) and small amount of other elements (Fig. S3c). Combined the XRD pattern and EDS analysis, the impure peaks could be roughly assigned to diffraction peaks of orthorhombic $NaAlSiO_4$ (PDF 77-1179) and Fe_2SiO_4 (PDF 71-1670). These impurity possibly formed from the mineralization reactions during the high temperature carbonization process. Generally, two typical broad XRD peaks centered about 26° and 43° are produced by active carbon materials. Herein, the absence of these peaks may be due to the high amorphous nature of the prepared carbons, which are also observed for other KOH-activated carbons we reported previous (All of the XRD patterns are obtained from the same XRD instrument) [10,49].

Raman spectroscopy has been a powerful characterization technique to analyze the structure of carbon materials. The Raman spectra show two well-known bands at 1341 cm^{-1} (D peak) and 1591 cm^{-1} (G peak) for activated carbons (Fig. 3b), reflection of disorder graphitic carbon, respectively [50,51]. The graphitic G peak (assigned to E2g vibrational modes) is attributed to the bond stretching of all sp^2 atoms in chains and rings; while, the D peak corresponds to the breathing mode of sp^2 atoms in rings characteristic of disorder and defect within the carbon matrix. The I_D/I_G values are determined to be 1.02, 1.02, 1.03 and 1.04 for BBC-1, BBC-2, BBC-3, and BBC-4, respectively, which further proved the amorphous structure of the prepared carbons. The electrical conductivities of the prepared carbon materials are between 23 and 40 mS cm^{-1}. The slight increase of I_D/I_G values and rough decrease of electrical conductivities indicates that the carbon structure becomes more amorphous under high KOH dosage.

The surface elemental compositions of BBCs were confirmed by EDS and XPS tests (Fig. 4). C, O and trace amount of N elements are determined in EDS mapping and their distribution are relative uniform (Fig. 4a). High resolution XPS were in progress to investigate the atom binding energy of the materials (Fig. 4b–e). The nitrogen and oxygen content are 0.8 and 11.9 at% for BBC-4, respectively (Table S1). The abundant presence of O functional groups in the prepared materials can facilitate the wettability of the electrode, leading to an effective mass transfer. The high resolution C1s spectrum can be marked into four peaks. The main peak centered at 284.7 eV are corresponds to carbon atoms single bonded to N, O, and the weak peaks in the range of 286.4–289 eV are correspond carbonyl, ester or carboxylic groupsy [52] (Fig. 4c). O1s scans show three peaks with varying contributions. The binding energies are 531.1, 532.4, and 533.4 eV which were assigned to quinone groups (O-I), phenol groups (O-II) and carboxyl groups (O-III), respectively (Fig. 4d) [53]. Peaks at 398.6 eV (N-6), 400.5 eV (N-5) and 401.2 eV (N-Q) are represent pyridinic N, pyrrolic N and quaternary N, respectively [54] (Fig. 4e). The high resolution XPS spectra of other samples give similar results (Fig. S4-S6).

3.2. Electrochemical performance in three aqueous electrolytes

The obtained BBCs were firstly investigated as the electrodes materials for supercapacitors in the most common KOH electrolyte (Fig. 5). CV measurements were firstly conducted to detect the electrochemical behaviors of the carbon materials. As shown in Fig. 5a, all the CV profiles obtained at 10 mV s^{-1} from −0.9 to 0 V show a typical rectangle shape, indicating all the investigated carbons store charge mainly via an electrochemical double layer capacitive mechanism [18,55,56]. As the sweep rate increases to 500 mV s^{-1}, CV curve of BBC-4 still remains nearly standard rectangular shape, indicating this material possesses excellent rate performance (Fig. 5b). As can be seen from Fig. 5c, the discharge time is roughly equal to the charging time, and the GCD curves approximately exhibit the isosceles triangle, indicating a high coulombic efficiency. The coulomb efficiencies are 91% at 0.6 A g^{-1}, 95% at 1 A g^{-1} and > 99% in 2–100 A g^{-1}, respectively (Fig. S7). Few irreversible chemical reactions reduce the coulomb efficiencies when the current density is low. From a low current density of 0.3 A g^{-1} up to a ultrahigh current density of 100 A g^{-1}, the electrode materials could be smoothly charged and discharged (Fig. S7). The low voltage drops at the initial of discharge curves are resulted from the good electrical conductivities of the prepared carbons (Table 1). According to the galvanostatic charge/discharge curves, the specific capacitances are calculated to 242, 281, 258 and 327 F g^{-1} for BBC-1, BBC-2, BBC-3 and BBC-4 at 0.2 A g^{-1}, respectively. At high current density, the electrolyte ions cannot diffuse into the micropores in time, the specific capacitances gradually decrease. However, BBC-4 shows the highest specific capacitance at all the test current densities, and still keeps 205 F g^{-1} at a very high current density of 100 A g^{-1}, responding to an outstanding retention ratio of 62.7% in range of 0.2–100 A g^{-1}. The excellent capacitive performance, especially the high rate performance, are attributed to the fast ionic transportation and charge transfer in the hierarchical pore texture.

Because alkaline electrolyte is easy to leak, so we further evaluated the capacitive performance of the prepared carbons in 1 M H_2SO_4 electrolyte with a two-electrode system. At low sweep rate of 10 mV s^{-1}, the CV curves approximate to rectangles, also demonstrating a main energy storage mechanism of EDLC (Fig. 6a). With the sweep rate increasing, the rectangles was more deformed than those in

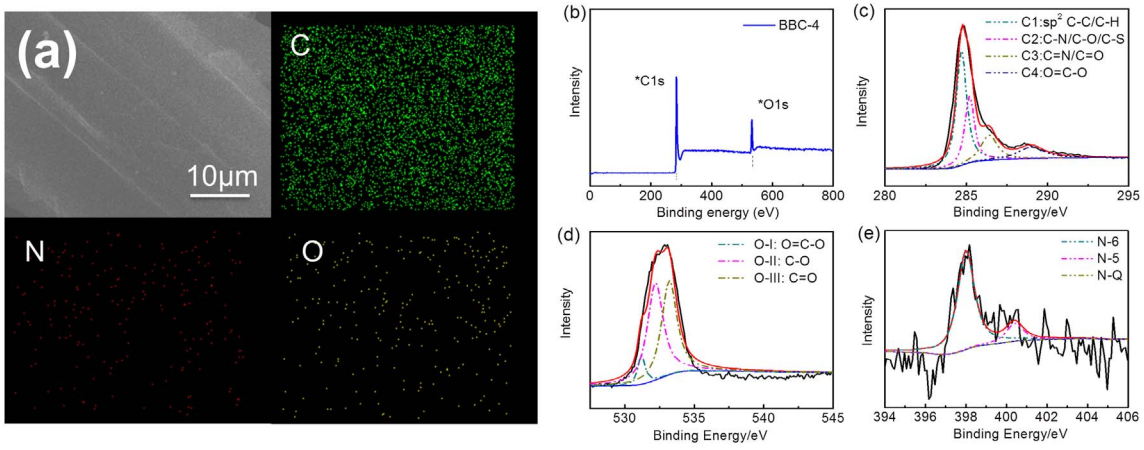

Fig. 4. (a) EDS mapping of BBC-4 sample; (b) XPS spectra, (c) C1s, (d) O1s, (e) N1s of BBC-4 sample.

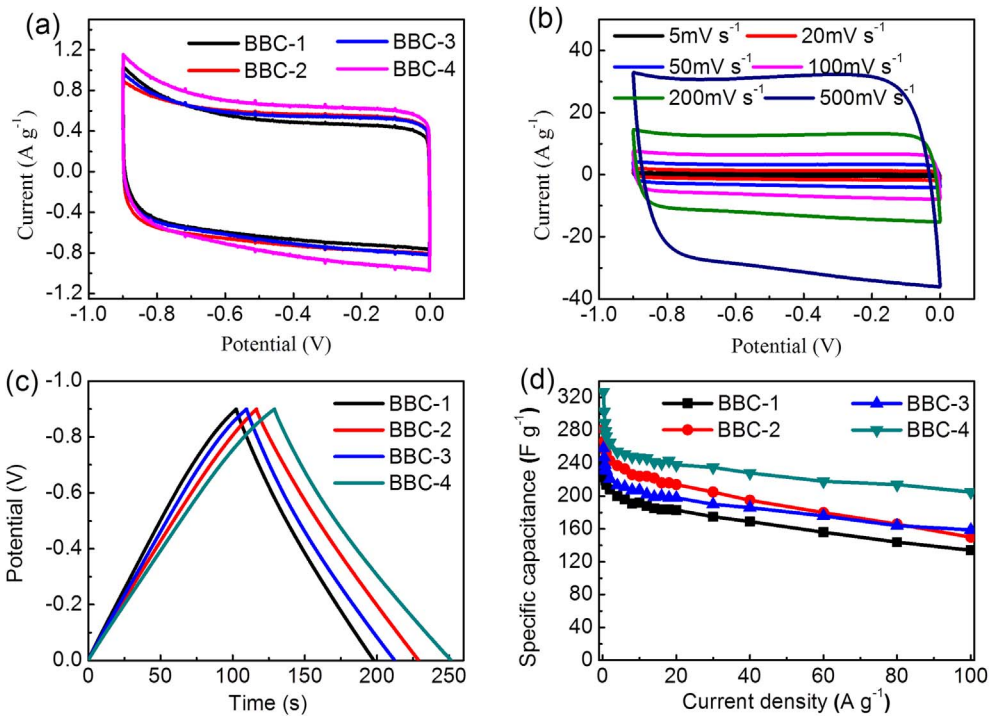

Fig. 5. Capacitive performance of BBCs in KOH electrolyte (a) CV curves at 10 mV s^{-1}, (b) CV curves of BBC-4 at 5–500 mV s^{-1}, (c) galvanostatic charge/discharge curves at 1 A g^{-1}, (c) specific capacitances at different current densities in the range of 0.2–100 A g^{-1}.

KOH electrolyte (Fig. 6b). The specific capacitances at the range of 0.2–60 A g^{-1} are determined by galvanostatic charge/discharge test (Fig. S8). As shown in Fig. 6d, BBC-4 also shows the best electrochemical performance, containing a high specific capacitance of 260 F g^{-1} at 0.2 A g^{-1}, the highest specific capacitance at high current densities (130 F g^{-1} at 60 A g^{-1}), and the highest retention ratio of 50% in the range of 0.2–60 A g^{-1}. It should be noted that the specific capacitance and rate performance are slightly lower than those in KOH electrolyte, which may be due to the low electrical conductivity and larger ion size of H_2SO_4 electrolyte.

It is well known that the energy densities of supercapacitor are proportional to the square of voltage window of supercapacitors. However, the operating voltage of supercapacitors based on KOH or H_2SO_4 electrolyte can reach only above 1 V, because water will decompose at higher voltage [57], thus limiting the energy densities of supercapacitors. The neutral Na_2SO_4 electrolyte has been very promising due to its advantages such as the high operation voltage and being environmentally friendly. We firstly investigated the capacitive performance of all the BBCs samples at 1.2 V. As shown in Fig. 7a and b, typical EDLC behaviors are determined. Fig. 7c presents that BBC-4

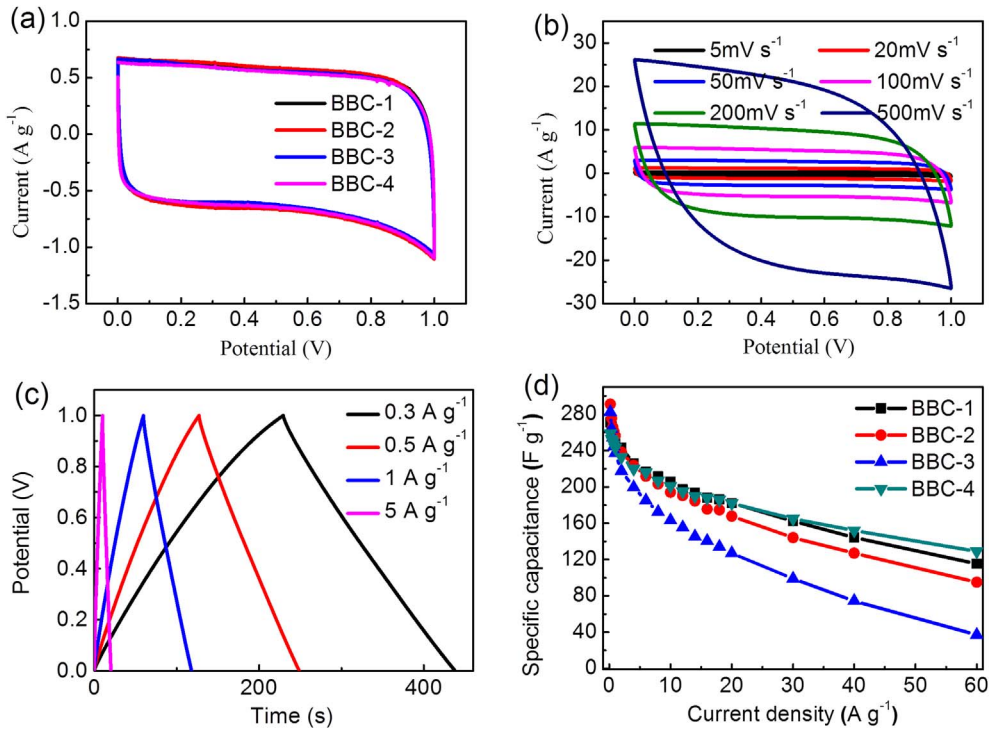

Fig. 6. Capacitive performance of the BBCs in H_2SO_4 electrolyte (a) CV curves at 10 mV s^{-1}, (b) CV curves of BBC-4 at 5–500 mV s^{-1}, (c) galvanostatic charge/discharge curves at 1 A g^{-1}, (d) specific capacitances at different current densities in the range of 0.2–60 A g^{-1}.

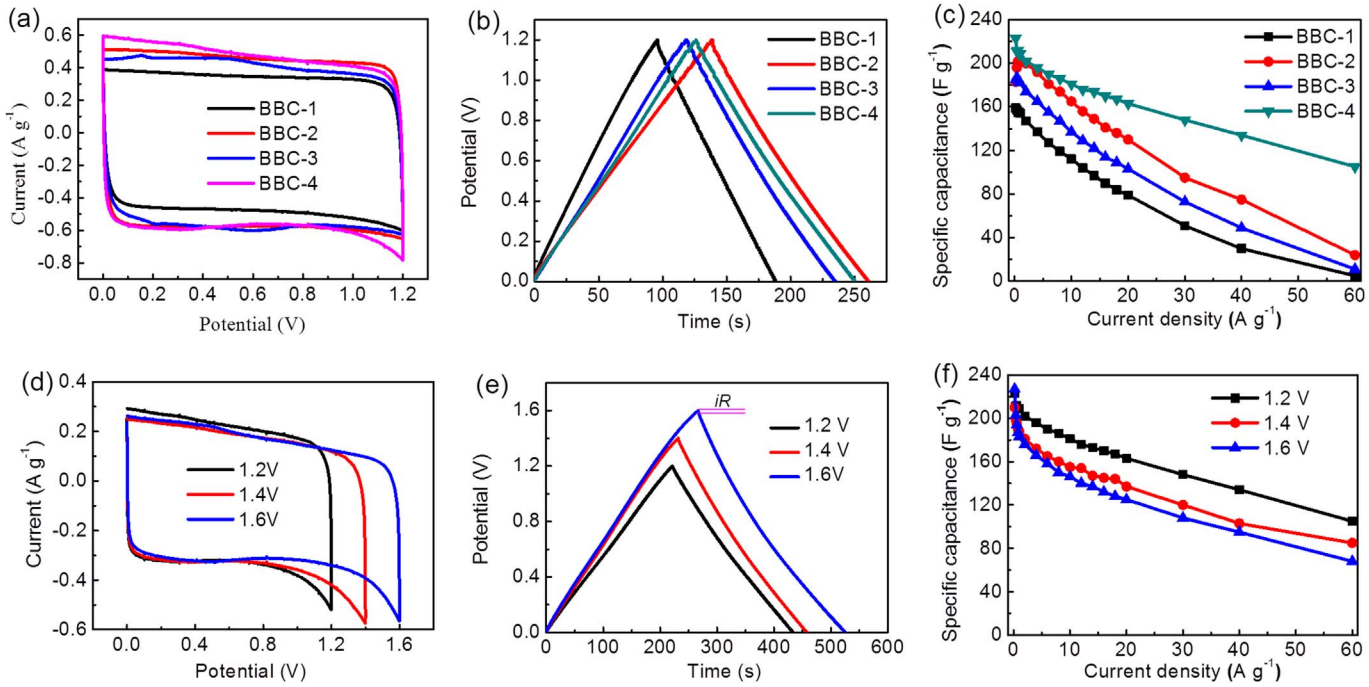

Fig. 7. Capacitive performance of the BBCs in Na_2SO_4 electrolyte (a) CV curves at 10 mV s^{-1}, (b) galvanostatic charge/discharge at 1 A g^{-1}, (c) specific capacitances at different current densities in the range of 0–1.2 V, (d) CV curves in different voltage windows at 5 mV s^{-1}, (e) galvanostatic charge/discharge curves at 0.3 A g^{-1}, (f) specific capacitances of BBC-4 at different voltage windows.

exhibits the best capacitive performance among the prepared carbon materials, which agree well with the results in KOH and H_2SO_4 electrolytes. These facts may be due to the complicated synergistic effect of its highest specific surface area, hierarchical porosity consisting of small micropores (0.5–1.0 nm), larger micropores (> 1.0 nm) and large amount of small mesopores (2.0–6.0 nm), and its higher oxygen content. Then, the electrochemical performance of BBC-4 at different work voltages are investigated separately (Fig. 7d–f, Fig. S9 and S10). Fig. 7d shows the CV curves of BBC-4 at different voltage windows from 1.2 to 1.6 V at a slow scan rate of 5 mV s^{-1}. All the curves possess a rectangular-like shape, and no apparent oxygen evolution reactions are observed. Isosceles triangle-liked charge/discharge curves with a low iR drop can be observed in Fig. 7e and S8. These facts indicate that this carbon material still maintain a good capacitance characterization and could steady work at a high voltage of 1.6 V. At a work voltage of 1.6 V, BBC-4 gives a very high specific capacitance of 227 F g^{-1} at 0.2 F g^{-1}, and still retains 68 F g^{-1} when the current density increases by 300 times, up to 60 A g^{-1}. This good consequence might be attribute to the collaborative effect of the hierarchical porosity and high specific surface area.

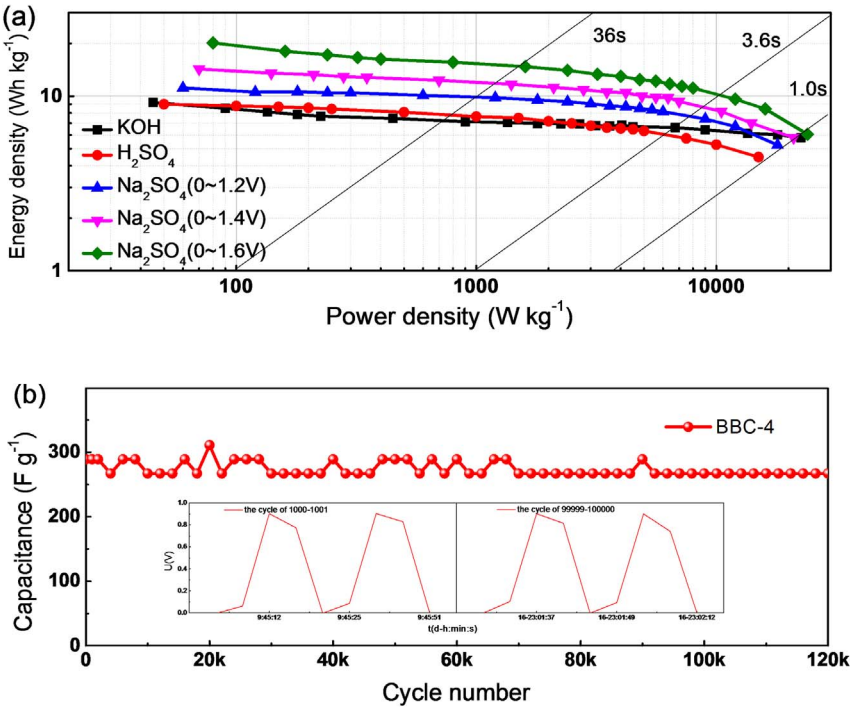

Fig. 8. (a) Ragone plots of BBC-4 in KOH, H_2SO_4 and Na_2SO_4 electrolytes, (b) long term stability test up to 120 000 cycles.

Table 2
Comparison with other biomass-based carbon materials.

Biomass	Activating method	S_{BET} (m^2 g^{-1})	Capacitance (F g^{-1})	Electrolyte	Ref.
biochar	KOH	2790	**327**	6 M KOH	This
			259	1 M H_2SO_4	work
			223	1 M Na_2SO_4	
wood	KOH	2925	250	6 M KOH	[32]
sunflower seed	KOH	1162	244	6 M KOH	[58]
	CO_2+KOH	2509	311	6 M KOH	
waste paper	KOH	526	180	6 M KOH	[59]
lignocellulosic	KOH	1100	161	6 M KOH	[60]
fish scale	KOH	2273	168	6 M KOH	[61]
cassava peel	KNO_3	1186	264	1 M H_2SO_4	[62]
pig bone	KOH	2157	185	6 M KOH	[63]
coffee endocarp	KOH	1050	176	1 M H_2SO_4	[64]

Fig. 8a shows the Ragone plots of BBC-4 in different test conditions. It could be seen that the energy density drops with the increase of power density, which means higher power export at lower energy density. Although the specific capacitances in Na_2SO_4 electrolyte are obviously lower than those in KOH and H_2SO_4 electrolytes, the BCC-4 delivers superior energy densities in Na_2SO_4 electrolyte due to its much higher work voltage (1.6 V). At a power density of 80 W kg^{-1}, a ultrahigh energy density of 20.2 Wh kg^{-1} is gained in Na_2SO_4 electrolyte. At a high power density of 24 000 W kg^{-1}, responding to a very small drain time of 1s, the energy density is still up to 6 Wh kg^{-1}. It should be noted that the energy densities are estimated only based on the weight of carbon materials. The practical energy densities will much decrease since the energy densities of a practical supercapacitor are also related to the mass proportion of carbon material in the total supercapacitor.

The cycle life is also an important requirement for supercapacitors. Fig. 8b shows the capacitance retention as a function of cycle number in KOH electrolyte. After very long continuous charge/discharge test up to 120 000 cycles (about 21 days), the supercapacitor still smoothly charge/discharge, and the active material of BBC-4 still retains 267 F g^{-1} at 5 A g^{-1}, about 92.4% of its initial value. We further carried out the long-term cyclic measurement of BBC-4 in H_2SO_4 and Na_2SO_4 electrolytes. As shown in Fig. S11a, c, after 10 000 cycles in H_2SO_4 electrolyte with a work voltage of 1 V, the retention rate is 86.7% with a small voltage drop. In Na_2SO_4 electrolyte, the performance of electrodes varied with the work voltage in the range of 1.2V-1.6 V (Fig. S11b). At a work voltage of 1.2 V, the retention ratio maintained at about 75% after 6000 cycles (Fig. S11d). At a higher work voltage of 1.4 or 1.6 V, the capacitance sharply decrease after 3000 cycles, and lost its most capacitance after about 9000 and 7500 cycles, respectively. In summary, the stability of the electrode material decreases as the charge voltage increases from 0.9 V of the KOH electrolyte to 1.6 V of the Na_2SO_4 electrolyte. The possible reasons may be (a) the amorphous structure of the prepared carbon is unstable at high work voltage, (b) the large surface and high-leveled oxygen-doping of the prepared carbon could catalyze the decompose of H_2O into O_2 at high work voltage, resulting in the oxidation of the carbon material. Furthermore, we observed the micromorphology of the BBC-4 carbon before and after 10 000 charge/discharge cycles in Na_2SO_4 electrolyte. As shown in Fig. S12d, after being pressed on the work electrode, lots of fibrous carbon particles collapsed into smaller particles. As shown in Fig. R12e-h, no obvious change of micromorphology is observed, the tubular channels and mesopores on their walls are still maintained, indicating that the pore texture is very stable during the long-term charge/discharge cycles.

Finally, we compared the capacitive performance of BBC-4 with other biomass-based carbon materials ever reported. As shown in Table 2, the specific capacitances of biochar-based carbons prepared here are much higher than that of carbon materials prepared from wood [32], sunflower seed [58], waste paper [59], lignocellulose [60], fish scale [61], cassava peel [62], pig bone [63], and coffee endocarp [64], further confirming the excellent performance of the BBCs prepared here.

4. Conclusions

Porous carbon materials are prepared to be electrode materials for supercapacitors by using corn straw biochar as precursor and KOH as activation agent. The prepared biochar-based carbon materials possess hierarchical micro-meso-macro porosity and very high specific surface areas. Due to synergetic effect of multi-leveled pores, the BBC-4 material shows excellent capacitive properties in the basic, acidic and neutral electrolytes, such as high specific capacitance up to 327 F g^{-1}, high rate performance, and high work voltage up to 1.6 V. The carbon material also possesses excellent long-term stability up to 120 000 cycles and remarkable energy density of 20.2 Wh kg^{-1}. The results of this work prove that the biochar-based porous carbons are very promising electrode material for supercapacitors. More importantly, we developed here opens up the new possibility of utilization of biochar into high value-added areas.

Acknowledgements

We are grateful for the financial supports by National Natural Science Foundation of China (NSFC21576158, 61604089 and 21576159) and Natural Science Foundation of Shandong Province (ZR2017JL014 and ZR2016AQ14).

Appendix A. Supplementary data

Supplementary data related to this article can be found at http://dx.doi.org/10.1016/j.jpowsour.2017.11.077.

References

[1] M. Salanne, B. Rotenberg, K. Naoi, K. Kaneko, P.-L. Taberna, C. Grey, B. Dunn, P. Simon, Nat. Energy 1 (2016) 16070.
[2] M.Q. Zhao, M. Torelli, C.E. Ren, M. Ghidiu, Z. Ling, B. Anasori, M.W. Barsoum, Y. Gogotsi, Nano Energy 30 (2016) 603–613.
[3] Y. Wu, M. Gong, M.C. Lin, C. Yuan, M. Angell, L. Huang, D.Y. Wang, X. Zhang, J. Yang, B.J. Hwang, Adv. Mater. 28 (2016) 9218–9222.
[4] X. Liang, A. Garsuch, L.F. Nazar, Angew. Chem. Int. Ed. 54 (2015) 3907–3911.
[5] L. Wang, J. Yu, X. Dong, X. Li, Y. Xie, S. Chen, P. Li, H. Hou, Y. Song, ACS Sustain. Chem. Eng. 4 (2016) 1531–1537.
[6] M.G. Hahm, A. Leela Mohana Reddy, D.P. Cole, M. Rivera, J.A. Vento, J. Nam, H.Y. Jung, Y.L. Kim, N.T. Narayanan, D.P. Hashim, C. Galande, Y.J. Jung, M. Bundy, S. Karna, P.M. Ajayan, R. Vajtai, Nano Lett. 12 (2012) 5616–5621.
[7] X.J. Li, W. Xing, J. Zhou, G.Q. Wang, S.P. Zhuo, Z.F. Yan, Q.Z. Xue, S.Z. Qiao, Chemistry 20 (2014) 13314–13320.
[8] A. Burke, Electrochimica Acta 53 (2007) 1083–1091.
[9] Y. Jin, K. Tian, L. Wei, X. Zhang, X. Guo, 4 (2016).

[10] J. Zhou, Z. Qiu, J. Zhou, W. Si, H. Cui, S. Zhuo, Electrochimica Acta 180 (2015) 1007–1013.
[11] Z.-Y. Sui, Q.-H. Meng, J.-T. Li, J.-H. Zhu, Y. Cui, B.-H. Han, J. Mater. Chem. A 2 (2014) 9891–9898.
[12] B. Zhu, K. Li, J. Liu, H. Liu, C. Sun, C.E. Snape, Z. Guo, J. Mater. Chem. A 2 (2014) 5481–5489.
[13] G.-P. Hao, W.-C. Li, D. Qian, G.-H. Wang, W.-P. Zhang, T. Zhang, A.-Q. Wang, F. Schüth, H.-J. Bongard, A.-H. Lu, J. Am. Chem. Soc. 133 (2011) 11378–11388.
[14] J. Liu, N.P. Wickramaratne, S.Z. Qiao, M. Jaroniec, Nat. Mater. 14 (2015) 763–774.
[15] S.J. Yang, M. Antonietti, N. Fechler, J. Am. Chem. Soc. 137 (2015) 8269–8273.
[16] H. Fan, W. Shen, ACS Sustain. Chem. Eng. 4 (2015) 1328–1337.
[17] Y. Liu, Z. Shi, Y. Gao, W. An, Z. Cao, J. Liu, ACS Appl. Mater. interfaces 8 (2016) 28283–28290.
[18] D. Yuan, J. Chen, S. Tan, N. Xia, Y. Liu, Electrochem. Commun. 11 (2009) 1191–1194.
[19] S. Chen, J. Duan, Y. Tang, S. Zhang Qiao, Chemistry 19 (2013) 7118–7124.
[20] J. Zhou, Z. Zhang, W. Xing, J. Yu, G. Han, W. Si, S. Zhuo, Electrochimica Acta 153 (2015) 68–75.
[21] B. Xu, Y. Chen, G. Wei, G. Cao, H. Zhang, Y. Yang, Mater. Chem. Phys. 124 (2010) 504–509.
[22] H. Deng, G. Zhang, X. Xu, G. Tao, J. Dai, J. Hazard. Mater. 182 (2010) 217–224.
[23] T. Wang, S. Tan, C. Liang, Carbon 47 (2009) 1880–1883.
[24] T.E. Rufford, D. Hulicova-Jurcakova, Z. Zhu, G.Q. Lu, Electrochem. Commun. 10 (2008) 1594–1597.
[25] Q.-Y. Li, H.-Q. Wang, Q.-F. Dai, J.-H. Yang, Y.-L. Zhong, Solid State Ionics 179 (2008) 269–273.
[26] L. Wei, G. Yushin, Nano Energy 1 (2012) 552–565.
[27] T.E. Rufford, D. Hulicova-Jurcakova, K. Khosla, Z. Zhu, Q.L. Gao, J. Power Sources 195 (2010) 912–918.
[28] S.I. Weijiang, W.U. Xiaozhong, W. Xing, J. Zhou, S.P. Zhuo, J. Inorg. Mater. 26 (2011) 107–112.
[29] W.-J. Si, X.-Z. Wu, W. Xing, J. Zhou, S.-P. Zhuo, J. Inorg. Mater. 26 (2011) 107–113.
[30] D. Kalderis, S. Bethanis, P. Paraskeva, E. Diamadopoulos, Bioresour. Technol. 99 (2008) 6809.
[31] H. Yin, B. Lu, Y. Xu, D. Tang, X. Mao, W. Xiao, D. Wang, A.N. Alshawabkeh, Environ. Sci. Technol. 48 (2014) 8101–8108.
[32] L. Chen, T. Ji, L. Brisbin, J. Zhu, ACS Appl. Mater. interfaces 7 (2015) 12230–12237.
[33] S. Zhao, C.-Y. Wang, M.-M. Chen, J. Wang, Z.-Q. Shi, J. Phys. Chem. Solids 70 (2009) 1256–1260.
[34] E. Taer, M. Deraman, I.A. Talib, A. Awitdrus, S.A. Hashmi, A.A. Umar, Int. J. Electrochem. Sci. 6 (2015) 3301–3315.
[35] A.M. Abioye, F.N. Ani, Renew. Sustain. Energy Rev. 52 (2015) 1282–1293.
[36] T. Kan, V. Strezov, T.J. Evans, Renew. Sustain. Energy Rev. 57 (2016) 1126–1140.
[37] L.R. Iverson, S. Brown, A. Prasad, H. Mitasova, G. Ajr, A.E. Lugo, Use of GIS for Estimating Potential and Actual Forest Biomass for Continental South and Southeast Asia, Springer New York, 1994.
[38] PASWR, (2003).
[39] M.I. Jahirul, M.G. Rasul, A.A. Chowdhury, N. Ashwath, Energies 5 (2012) 4952–5001.
[40] M. Balat, M. Balat, E. Kırtay, H. Balat, Energy Convers. Manag. 50 (2009) 3147–3157.
[41] M.J.A. †, , S.G.A. †, Xiangfeng Dai, Brent Shimizu, M. S. Tam, M. Grønli‡, Industrial Eng. Chem. Res., 39 (2000) 4024–4031.
[42] A. M, R. AU, L. JE, Z. M, B. N, M. D, V. M, L. SS, O. YS, Chemosphere 99 (2014) 19–33.
[43] Z.H. Li, S.J. Li, J. Zhou, T.T. Zhu, H.L. Shen, S.P. Zhuo, ACTA PHYSICO-CHIMICA SIN. 31 (2015).
[44] T. Wigley, A.C.K. Yip, S. Pang, Energy 109 (2016) 481–494.
[45] E. Raymundo-Pinero, P. Azais, T. Cacciaguerra, D. Cazorla-Amorós, A. Linares-Solano, F. Béguin, Carbon 43 (2005) 786–795.
[46] D. Lozano-Castello, J. Calo, D. Cazorla-Amoros, A. Linares-Solano, Carbon 45 (2007) 2529–2536.
[47] J. Zhou, Z. Li, W. Xing, H. Shen, X. Bi, T. Zhu, Z. Qiu, S. Zhuo, Adv. Funct. Mater. 26 (2016) 7955–7964.
[48] J. Wang, S. Kaskel, J. Mater. Chem. 22 (2012) 23710–23725.
[49] J. Zhou, T. Zhu, W. Xing, Z. Li, H. Shen, S. Zhuo, Electrochimica Acta 160 (2015) 152–159.
[50] S.H. Park, S.M. Bak, K.H. Kim, J.P. Jegal, S.I. Lee, J. Lee, K.B. Kim, J. Mater. Chem. 21 (2010) 680–686.
[51] C.Y. Su, Y. Xu, W. Zhang, J. Zhao, X. Tang, C.H. Tsai, L.J. Li, Chem. Mater. 21 (2011) 5674–5680.
[52] X.Y. Chen, C. Chen, Z.J. Zhang, D.H. Xie, X. Deng, J.W. Liu, J. Power Sources 230 (2013) 50–58.
[53] S. Biniak, G. Szymański, J. Siedlewski, A.Ś.j.m. tkowski, Carbon 35 (1997) 1799–1810.
[54] R.J.J. Jansen, H.V. Bekkum, Carbon 33 (1995) 1021–1027.
[55] J. Yang, H. Wu, M. Zhu, W. Ren, Y. Lin, H. Chen, F. Pan, Nano Energy 33 (2017) 453–461.
[56] M.F. El-Kady, V. Strong, S. Dubin, R.B. Kaner, Science 335 (2012) 1326–1330.
[57] B.P. Bakhmatyuk, A.S. Kurepa, (2012).
[58] X. Li, W. Xing, S. Zhuo, J. Zhou, F. Li, S.Z. Qiao, G.Q. Lu, Bioresour. Technol. 102 (2011) 1118–1123.
[59] D. Kalpana, S. Cho, S. Lee, Y. Lee, R. Misra, N. Renganathan, J. Power Sources 190 (2009) 587–591.
[60] P. González-García, T.A. Centeno, E. Urones-Garrote, D. Ávila-Brande, L.C. Otero-Díaz, Appl. Surf. Sci. 265 (2013) 731–737.
[61] W. Chen, H. Zhang, Y. Huang, W. Wang, J. Mater. Chem. 20 (2010) 4773–4775.
[62] A.E. Ismanto, S. Wang, F.E. Soetaredjo, S. Ismadji, Bioresour. Technol. 101 (2010) 3534–3540.
[63] W. Huang, H. Zhang, Y. Huang, W. Wang, S. Wei, Carbon 49 (2011) 838–843.
[64] J.M. Nabais, J.G. Teixeira, I. Almeida, Bioresour. Technol. 102 (2011) 2781–2787.